Journal of Nuclear Materials 510 (2018) 187–192

Contents lists available at ScienceDirect

Journal of Nuclear Materials

journal homepage: www.elsevier.com/locate/jnucmat

Microstructural response of He^+ irradiated $FeCoNiCrTi_{0.2}$ high-entropy alloy

Da Chen [a], Y. Tong [a, b], J. Wang [a, b], B. Han [a, b], Y.L. Zhao [a], F. He [a], J.J. Kai [a, b, c, *]

[a] Department of Mechanical and Biomedical Engineering, City University of Hong Kong, Hong Kong, China
[b] Centre for Advanced Nuclear Safety and Sustainable Development, City University of Hong Kong, Hong Kong, China
[c] Department of Engineering and System Science, National Tsing-Hua University, Hsinchu, 30013, Taiwan

HIGHLIGHTS

- Helium bubbles and faulted dislocation loops formed in the He^+ irradiated $FeCoNiCrTi_{0.2}$ HEA.
- The faulted type defects are energetically favorable in $FeCoNiCrTi_{0.2}$ HEA.
- The low stacking fault energy could suppress the transformation of dislocation loops.

ARTICLE INFO

Article history:
Received 29 May 2018
Received in revised form
1 August 2018
Accepted 5 August 2018
Available online 7 August 2018

Keywords:
High-entropy alloy
Helium bubbles
Faulted dislocation loops
Stacking fault energy

ABSTRACT

In the He^+ irradiated $FeCoNiCrTi_{0.2}$ high-entropy alloy (HEA), radiation-induced defects including helium bubbles and faulted dislocation loops were characterized by transmission electron microscopy. Compared with other face-centered cubic alloys irradiated in similar conditions, we found that the faulted loops in the $FeCoNiCrTi_{0.2}$ HEA have a much large size, whereas the perfect loops were rarely detected. Our results reveal that the faulted-type defect structure is more energetically favorable in the $FeCoNiCrTi_{0.2}$ HEA, whereas the transformation of the faulted to perfect dislocation loops was suppressed. For the underlying mechanism, we propose that the low stacking fault energy can stabilize the faulted planar defects during irradiation.

1. Introduction

High-entropy alloys (HEAs), as emerging alloys composed with four or more principal elements in equal-molar or near equal-molar fraction [1], open a new way to design alloys and draw great attention in material science community. Due to their excellent mechanical properties [2,3], great corrosion resistance [4], strong oxidation resistance [5,6], and promising radiation damage tolerance [7–12], HEAs have been proposed as the candidate for structural materials in advanced nuclear systems. Currently, the radiation responses of HEAs under heavy ions or self-ions bombardment have been well studied [7–12]. The great phase stability of $Al_xCoCrFeNi$ HEAs under a very high damage level of ~100 dpa has been demonstrated by Xia et al. [7], and it was explained by the unique effect of HEAs, i.e., high mixing entropy. Kumar et al. found that [8] Fe–Ni–Mn–Cr HEA has better radiation resistance than Fe–Cr–Ni austenitic stainless steels under Ni ion irradiation up to 10 dpa in a temperature range from 400 °C to 700 °C, by showing smaller dislocation loops and undetectable voids. Moreover, Lu et al. found that [9] with increasing compositional complexity in single-phase concentrated solid-solution alloys, the growth of the radiation-induced defects was delayed and the radiation-induced segregation (RIS) was significantly suppressed. He et al. [13] also investigated the elemental segregation in several HEAs subjected to 1250 kV electron irradiations, and they found that the actively segregating elements are alloy-specific, which could be rationalized based on the atomic size difference and enthalpy of mixing between the alloying elements. Recently, Chen et al. [14] and Yan et al. [15] investigated the helium behavior in the FeCoNiCr HEA from different perspectives, and they both found that the FeCoNiCr HEA shows a better bubble formation resistance. For the underlying mechanism of HEAs' radiation

* Corresponding author. Department of Mechanical and Biomedical Engineering, City University of Hong Kong, Hong Kong, China.
E-mail address: jijkai@cityu.edu.hk (J.J. Kai).

https://doi.org/10.1016/j.jnucmat.2018.08.006
0022-3115/

tolerance, Zhang et al. [11] conducted *ab initio* electronic structure calculations and physical property measurements, and found that the chemical complexity can cause a substantial reduction in electron mean free path and orders of magnitude decrease in electrical and thermal conductivities, which subsequently suppress the evolution of defects.

Most of above-mentioned researches are focused on the effect of compositional complexity on the radiation resistances of HEAs. The correlation between their intrinsic properties and the evolution of radiation-induced defects is still unclear. For example, the low stacking fault energy (SFE) of some HEAs has been deemed as the culprit of their unique deformation mechanism [16], whether it will make a different microstructural response in radiation circumstance? Moreover, the microstructural response of HEAs under He^+ irradiation has not been fully studied, which is very important for HEAs' application in nuclear system [17,18]. Thus, from both scientific interests and potential applications, we added 0.2 M ratio of Ti in the FeCoNiCr matrix to form a new solid solution HEA of $FeCoNiCrTi_{0.2}$, which is expected to have a lower SFE than the parent alloy. Its microstructural evolution under He^+ irradiation at elevated temperature was thoroughly investigated. Our results show that the behavior of radiation-induced dislocation loops was significantly influenced by SFE.

2. Experimental

The alloy with a composition of $FeCoNiCrTi_{0.2}$ was produced by arc melting Fe, Co, Ni, Cr and Ti metals with high purity (>99.9%) in an argon atmosphere. Then the drop-casted sample was homogenized at 1373 K for 5 h and then water quenched to get a solid solution state. As a novel material, the crystalline structure of the pristine $FeCoNiCrTi_{0.2}$ HEA was firstly examined. Fig. 1 shows the X-ray diffraction (XRD) pattern and its microstructure characterized by scanning electron microscope (SEM). It can be seen that the solid-solution $FeCoNiCrTi_{0.2}$ HEA has only one phase with face-centered cubic (FCC) structure, and its average grain size was measured as ~180 μm.

The irradiation experiment was conducted at Accelerator Laboratory, National Tsing Hua University. The specimens were irradiated by 275 keV He ions to a fluence of 5.14×10^{20} ions/m^2 at 400 °C; during irradiation, the ion flux was controlled as ~1.84×10^{16} ions/m^2s and the test chamber pressure was maintained below 10^{-6} torr. Following irradiation, the cross-sectional transmission electron microscopy (TEM) sample shown in Fig. 2a was prepared by focused ion beam (FIB) lift-out techniques using a FEI Scios Dual Beam system. In order to remove the artificial damage induced by FIB, the TEM foil sample was cleaned by Gatan Model 695 Precision Ion Polishing System (PIPS II Pro) at 500 V prior to TEM characterization. A JEOL-2100F TEM operated at 200 kV was employed to characterize the radiation-induced defects.

The stopping and range of ions in matter program (SRIM-2010) [19] was used to predict damage level and He^+ distribution. According to suggestions from Stoller et at. [20], the quick Kinchin-Pease mode was adopted in this simulation and the displacement energy was set to 40 eV for all target elements. In Fig. 2b, the radiation damage and helium concentration profiles calculated from SRIM were plotted together with the cross-sectional TEM image. It shows that the maximum damage and peak of helium concentration occurred in the depth range from 500 nm to 700 nm, and their average values in this region can reach ~1 dpa and ~25000 appm, respectively. In the TEM image, a damage band showing different contrast was observed in this range, which is consistent with the prediction by SRIM.

3. Results and discussions

It has been demonstrated that the addition of Ti in the FeCoNiCr HEA usually introduces the intermetallic phase with $L1_2$ structure at intermediate temperatures [21,22]. Therefore, before the microstructure characterization of radiation-induced defects, we conducted a series of selected-area electron diffraction (SAED) experiments along the irradiated depth to detect the phase stability of HEA during irradiation. An inset image in Fig. 2 (b) displays a SAED pattern (taken along the zone axis of ⟨011⟩) obtained from the irradiated region. We found that the very faint superlattice spots appear among the fcc-matrix diffraction spots, indicating that the $L1_2$ ordering structure was formed during elevated-temperature irradiation. However, the superlattice diffraction spots from $L1_2$ phase was also observed in the regions far beyond the radiation damage layer, and thus the slightly ordering process was caused by annealing at 400 °C rather than the effect of He^+ irradiation. Then, the distribution of radiation-induced defects was examined from the TEM sample surface to the irradiation depth. The results show that the defects including helium bubbles and dislocation loops have a depth distribution, which strongly depends on the radiation damage (dpa) and implanted helium concentration. For example, the radiation-induced defects were mainly observed in the depth range from ~400 nm to ~780 nm, corresponding to the peak damage region. Below and above these depths, few defects (either He bubbles or dislocation loops) were detected. Hence, the following analysis on the radiation induced defects was all conducted in the peak damage region.

In Fig. 3, a series of kinetic two-beam bright field (BF) images and the corresponding weak beam dark field (WBDF) images were taken from the same region, and these images with three different

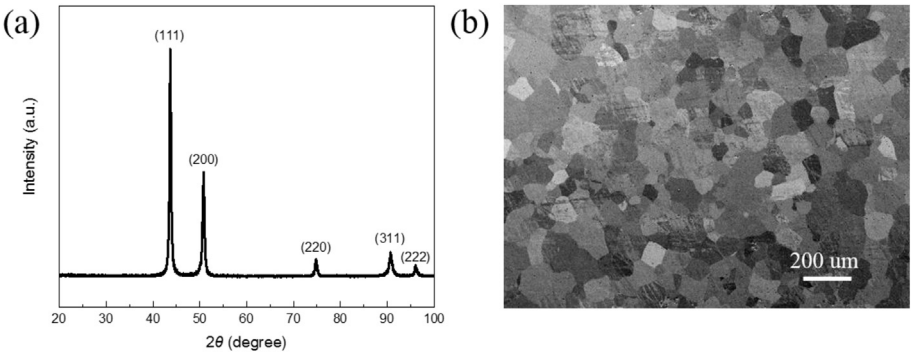

Fig. 1. (a) X-ray diffraction pattern and (b) SEM image of the $FeCoNiCrTi_{0.2}$ HEA in the solid solution state.

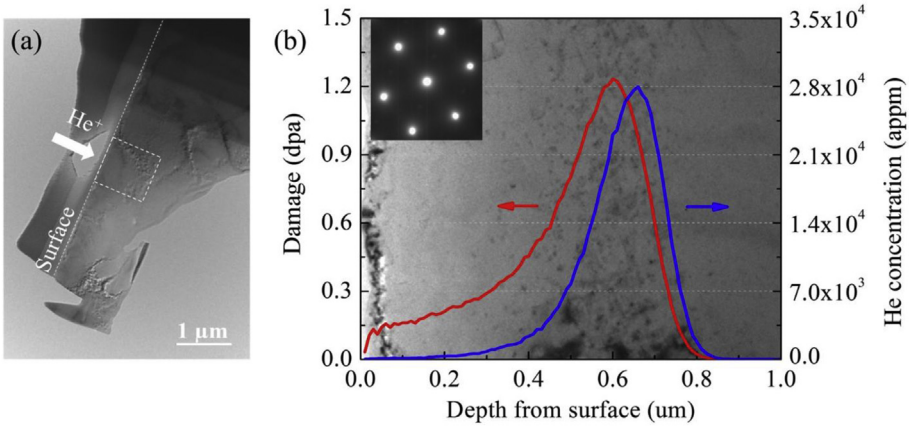

Fig. 2. (a) An overview of the TEM sample fabricated from the He^+ irradiated $FeCoNiCrTi_{0.2}$ HEA. (b) The damage and helium concentration profiles overlapped with a cross-sectional TEM image.

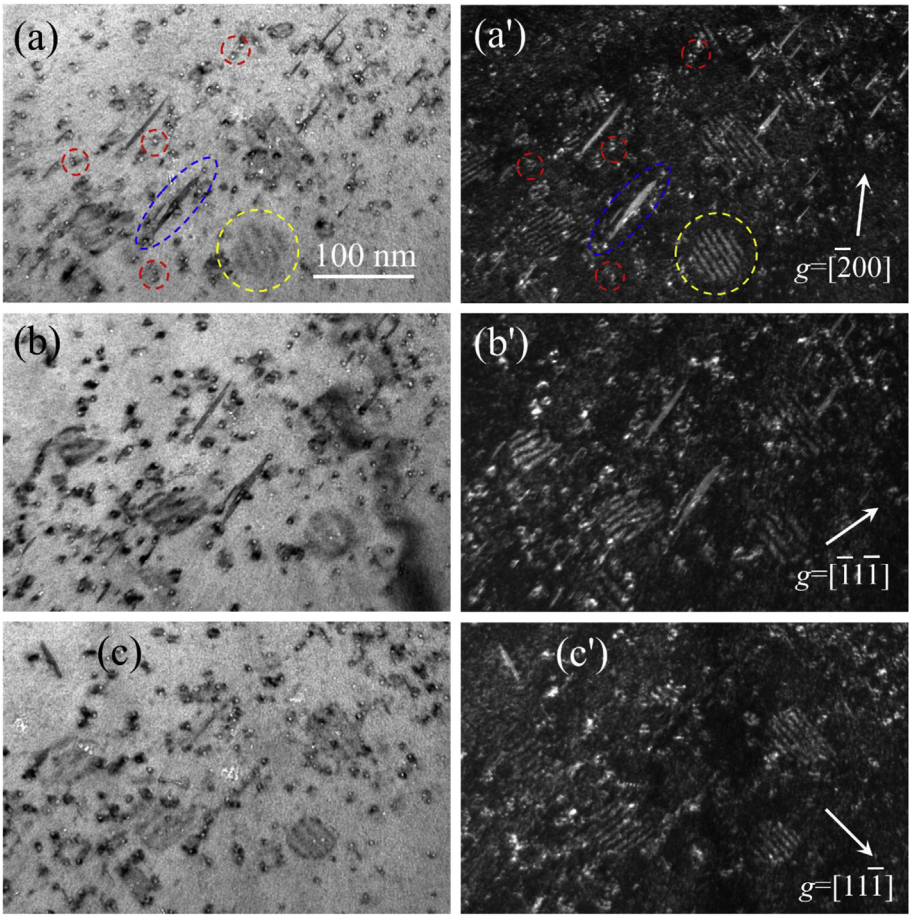

Fig. 3. The TEM images of radiation-induced defects in the He^+ irradiated $FeCoNiCrTi_{0.2}$ HEA. The under-focus BF images (a), (b), (c) were taken in kinetic two beam condition with different g vector, the corresponding WBDF images of (a'), (b'), (c') were taken at g (3g) condition, and the beam direction was along the zone axis of [011]. The helium bubbles and the associated strain field are marked by red circles, the edge-on faulted dislocation loops are marked by blue circles, and the non-edge-on faulted dislocation loops are marked by yellow circles. (For interpretation of the references to colour in this figure legend, the reader is referred to the Web version of this article.)

diffraction *g* vectors were used to distinguish different radiation-induced defects. Based on the Fresnel contrast mechanism, helium bubbles marked by red circles were characterized as white spots in the under-focus Fig. 3a, b, and 3c. The random distribution of helium bubbles implies a homogeneous nucleation process during the He^+ irradiation. Statistically, we analyzed the mean diameter of helium bubbles as 3.96 ± 0.61 nm from at least 5 representative TEM images, and their number density can reach ~$3.0 \times 10^{22}/m^3$ when the thickness of TEM sample was measured as ~80 nm by convergent beam electron diffraction (CBED) technique. Thus, the volume swelling of He^+ irradiated $FeCoNiCrTi_{0.2}$ HEA was determined as ~0.1% in the peak damage region. Meanwhile, the

dark-ring contrast surrounding individual bubble or bubble group was all observed in different tilting conditions, and they are independent of the focus condition. So this contrast should be induced by strain field. The WBDF images of Fig. 3', b', c' further verified that the strain field indeed exist at the position where helium bubbles appear in BF images. It has been suggested that [23] when the irradiation temperature is below than $0.5T_m$ and the ratio of He/dpa is very high, the pressure of helium bubbles can be close to the mechanical limit at which the matrix would yield by plastic deformation. Considering the irradiation condition in our case, this strain field contrast is likely caused by the high pressure inside the bubbles. Similarly, this strain field has been reported in 316L austenitic steel [24], which was implanted with 10 keV helium ions to 1×10^{15} cm^{-2} at 550 °C, and they suggest that the pressure inside of bubbles may exceed the equilibrium pressure of a few GPa.

Besides helium bubbles and their surrounding strain fields, the significant faulted dislocation loops are observed in Fig. 3. In the image taken along the zone axis of [011], the edge-on faulted dislocation loops were circled by blue dash lines, the non-edge-on loops were circled by the yellow ones, the visible parallel fringes inside loops are the signature of stacking fault. In Fig. 4, the high resolution TEM (HRTEM) images clearly reveal the local atomic arrangement of the faulted dislocation loops. The extra atomic plane marked by the red dash line in the magnified images of Fig. 4 a, d, indicates that the dislocation loops are indeed the interstitial type with the Burgers vector of $1/3\langle 111\rangle$. Also, the WBDF images (Fig. S1 in supplemental materials) taken at two opposite g vectors (based on the inside-outside mechanism [25]) revealed the varying contrasts of non-edge-on faulted loops, demonstrating that these loops are the nature of interstitial-type with the extrinsic character. These observations suggest that the self-interstitial atoms (SIAs) produced by displacement damage would agglomerate and precipitate into an additional layer on the {111} plane, so that the stacking sequence changed from CABCAB … to CAB|A|CAB, which is a typical structure of extrinsic stacking fault. The underlying mechanism of such microstructural response in He^+ irradiated $FeCoNiCrTi_{0.2}$ HEA is closely related to the evolution of point defects. During irradiation, most of the *Frenkel* pairs produced by energetic displacement cascade would recombine and annihilate, whereas the residual point defects (vacancies and interstitials) would diffuse and further evolve into defects with different geometrical configuration and energy state [26]. In our case, due to the low solubility of He in metals, the incident He could easily incorporate with vacancies to form a stable bubble nucleus, which could further grow through absorbing more He and vacancies. On the other hand, in order to reduce system energy, interstitials would coalesce and precipitate into planar defects, e.g. faulted dislocation loops. This is why the He bubbles coexist with interstitial faulted loops in our sample.

Fig. 5a shows the size distribution of dislocation loops analyzed from 5 different regions in He^+ irradiated $FeCoNiCrTi_{0.2}$ HEA. For this statistical analysis, at least 80 faulted loops were measured, and the lower limit of loop size was fixed in ~10 nm (the edge-on type faulted loops could be resolved at such small scale). Their mean diameter is ~45 nm, and the maximum value can reach 110 nm. We also can see that the size of faulted dislocation loops has a wide distribution, which might be related to the dynamic process of defect evolution. At the low damage level of ~1 dpa, the dislocation loop nucleation and growth might occur concurrently, and the growth of dislocation loop has not reach to a "saturation" stage. Moreover, through careful TEM investigation in different titling conditions, the unfaulted dislocation loops (perfect loops) with the Burgers vector of $1/2\langle 011\rangle$ and even the dislocation lines or their segments are rarely observed in Fig. 3. As suggested by Zinkle [27], during prolonged irradiation above temperature regime where SIAs and vacancies are mobile, the dislocation loop unfaulting usually occurs and these loops will finally evolve into the dislocation network structure. Thus, our observations in He^+ irradiated $FeCoNiCrTi_{0.2}$ HEA indicate that in such irradiation condition, the faulted dislocation loops could grow continuously and did not transform into the perfect ones, according to the known reaction [27]:

$$\frac{a}{3}\langle 111\rangle + \frac{a}{6}\langle 112\rangle = \frac{a}{2}\langle 011\rangle \quad (1)$$

In order to evaluate the dislocation loop formation in our case, the microstructural response of He^+ irradiated FeCoNiCr alloy at 400 °C was compared [14]. Here, we focused on the dislocation loop behavior, as shown in supplemental materials of Fig. S2. The FeCoNiCr parent alloy has much smaller dislocation loops with an average diameter of ~20 ± 10 nm. Furthermore, we surveyed the dislocation loop formation in several stainless steels which were all irradiated at 400 °C [28–31], and summarized their mean diameters as a function of dose, as show in Fig. 5b. Obviously, the

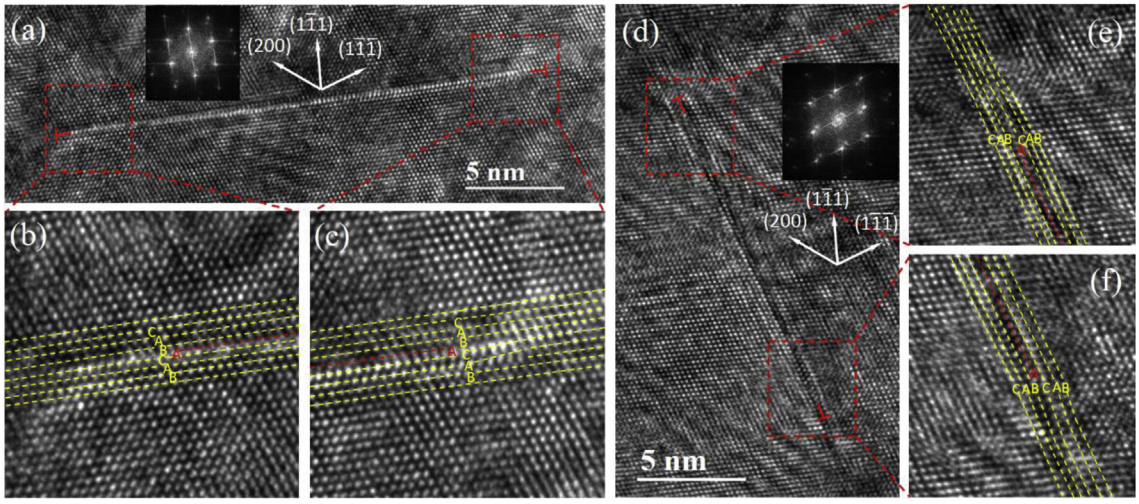

Fig. 4. HRTEM images of the faulted dislocation loops in the He^+ irradiated $FeCoNiCrTi_{0.2}$ HEA. The faulted loops in (a) and (d) are both identified as interstitial type, and the extra plane in (a) are magnified in (b), (c), the same as (e) and (f) for (d).

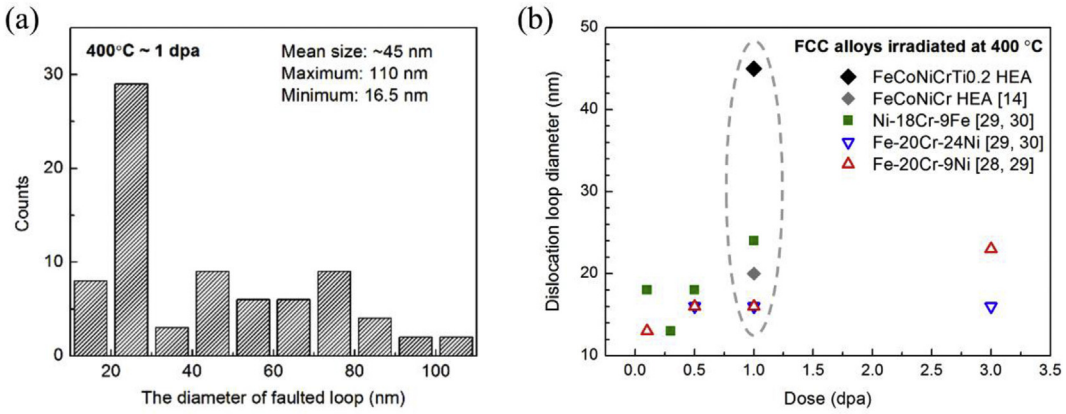

Fig. 5. (a) Size distribution of the faulted dislocation loops in the He^+ irradiated $FeCoNiCrTi_{0.2}$ HEA. (b) The mean diameter of dislocation loops reported in different FCC alloys was summarized as a function of dose.

faulted dislocation loops in our case have a much larger size. These comparisons imply that the faulted dislocation loops are more energetically favorable in $FeCoNiCrTi_{0.2}$ HEA, and the mentioned evolution of perfect or unfaulted dislocation was suppressed. Similarly, this phenomenon has also been reported in single-phase concentrated solid-solution alloys by Lu et al. [9], and they found that under the Ni^+ irradiation at 773 K, the fraction of faulted type in all dislocation loops was increased to 17%, 34% and 52% in the NiCoFe, NiCoFeCr and NiCoFeCrMn alloys, respectively; they suggest that the incubation period for the faulted to perfect loop transformation was extended in more complex alloy. Instead, our observations suggest that it should be attributed to their low stacking fault energy (SFE) [32].

Density functional theory calculations and experiments reveal that the SFE of HEAs increase with temperature, but the SFE of the FeCoNiCr HEA at 400 °C has not been reported. Here, we determined the SFEs based on the method provided by Hull and Bacon [33], i.e. characterizing the size of Frank dislocation loops by TEM. In their method, the energy difference ΔE between the Frank dislocations loop containing the stacking fault and the perfect loop could be expressed as follows [33]:

$$\Delta E = \pi r^2 \gamma - \frac{rGa^2}{24} \cdot \frac{2-\nu}{1-\nu} \ln\left(\frac{2r}{r_0}\right) \quad (2)$$

Where r is the radius of faulted loop, γ is the SFE, G is the shear modulus, a is the lattice constant, ν is the Poisson's ratio, and r_0 is the dislocation core radius. So when the energy of faulted loop larger than that of the perfect one, i.e., $\Delta E>0$, the unfaulting reaction of dislocation loop would happen. For our situation, there is no perfect loop observed, which means $\Delta E<0$, so the following relation could be derived:

$$\gamma < \frac{Ga^2}{24\pi r} \cdot \frac{2-\nu}{1-\nu} \ln\left(\frac{2r}{r_0}\right) \quad (3)$$

Substitute $G=72$ GPa (adopted from the data of FeCoNiCr at 673 K [34]), $a=0.3587$ nm (Rietveld refinement from $FeCoNiCrTi_{0.2}$ XRD data), $\nu=0.33$ and $r_0=0.5$ nm [33]. As the largest radius of faulted loop in $FeCoNiCrTi_{0.2}$ is ~55 nm, the upper limit of its SFE could be estimated as ~30 mJ/m^2 at 400 °C. Similarly, the SFE of FeCoNiCr alloy should be less than ~80 mJ/m^2 when the largest faulted loop was measured as ~30 nm in diameter. For stainless steels with a diameter of ~30 nm for the largest faulted loop [35], their SFE was estimated as ~80 mJ/m^2, and consistently the unfaulting reaction happened. Thus, the adding of minor Ti could significantly decrease the SFE of the FeCoNiCr matrix, and such effect was also reported in Ni-based superalloys [36].

The low SFE plays an important role in the evolution of both deformation defects and radiation defects. Many studies have shown that the extraordinary mechanical performance of the low SFE HEAs was due to the ease of mechanical twinning or the formation of stacking faults [37]. In the radiation scenario, when the SIAs produced by displacement damage are trapped by the nucleated faulted loops, the low SFE of HEA can stabilize these faulted planar defects and enable them to grow. Since the faulted dislocation loops have the Burgers vector of $1/3\langle 111\rangle$ vertical to the slip planes, they are usually sessile dislocations, which is detrimental to the ductility of the HEAs. However, as mentioned before, the low SFE can introduce mechanical twinning and/or stacking faults, which might alleviate the radiation-induced hardening. The impact of these faulted structure on the HEAs' mechanical properties still need further investigation.

In summary, the solid-solution $FeCoNiCrTi_{0.2}$ HEA was irradiated by 275 keV He^+ at 400 °C. TEM characterization revealed that the high-pressure helium bubbles surrounded by strain fields formed at the peak damage region, and meanwhile the interstitial Faulted dislocation loops of 1/3<111> were also formed. Distinct from the perfect dislocation loops observed in the austenitic steels irradiated under a similar condition, the faulted loops in the $FeCoNiCrTi_{0.2}$ HEA have an abnormal larger size while the perfect loop was rarely detected. These results imply that the faulted dislocation loops are more energetically favorable in the $FeCoNiCrTi_{0.2}$ HEA, and the low SFE can suppress the dislocation transformation from the faulted type to the perfect one. Overall, our study provides insights on the effect of SFE on the evolution of radiation-induced defects.

Acknowledgement

This work was supported by Hong Kong Research Grant Council (RGC) [Grant No. CityU 11212915].

Appendix A. Supplementary data

Supplementary data related to this article can be found at https://doi.org/10.1016/j.jnucmat.2018.08.006.

References

[1] J.W. Yeh, S.K. Chen, S.J. Lin, J.Y. Gan, T.S. Chin, T.T. Shun, C.H. Tsau, S.Y. Chang, Nanostructured high-entropy alloys with multiple principal elements: novel alloy design concepts and outcomes, Adv. Eng. Mater. 6 (5) (2004) 299–303.

[2] Z. Li, K.G. Pradeep, Y. Deng, D. Raabe, C.C. Tasan, Metastable high-entropy dual-phase alloys overcome the strength–ductility trade-off, Nature 534 (7606) (2016) 227–230.
[3] B. Gludovatz, A. Hohenwarter, D. Catoor, E.H. Chang, E.P. George, R.O. Ritchie, A fracture-resistant high-entropy alloy for cryogenic applications, Science 345 (6201) (2014) 1153–1158.
[4] M.-H. Tsai, J.-W. Yeh, High-entropy alloys: a critical review, Materials Research Letters 2 (3) (2014) 107–123.
[5] W. Kai, C.C. Li, F.P. Cheng, K.P. Chu, R.T. Huang, L.W. Tsay, J.J. Kai, The oxidation behavior of an equimolar FeCoNiCrMn high-entropy alloy at 950°C in various oxygen-containing atmospheres, Corrosion Sci. 108 (Supplement C) (2016) 209–214.
[6] W. Kai, F.P. Cheng, C.Y. Liao, C.C. Li, R.T. Huang, J.J. Kai, The oxidation behavior of the quinary FeCoNiCrSix high-entropy alloys, Mater. Chem. Phys. 210 (2017) 362–369.
[7] S. Xia, M.C. Gao, T. Yang, P.K. Liaw, Y. Zhang, Phase stability and microstructures of high entropy alloys ion irradiated to high doses, J. Nucl. Mater. 480 (2016) 100–108.
[8] N.A.P.K. Kumar, C. Li, K.J. Leonard, H. Bei, S.J. Zinkle, Microstructural stability and mechanical behavior of FeNiMnCr high entropy alloy under ion irradiation, Acta Mater. 113 (2016) 230–244.
[9] C. Lu, T. Yang, K. Jin, N. Gao, P. Xiu, Y. Zhang, F. Gao, H. Bei, W.J. Weber, K. Sun, Y. Dong, L. Wang, Radiation-induced segregation on defect clusters in single-phase concentrated solid-solution alloys, Acta Mater. 127 (2017) 98–107.
[10] T. Yang, S. Xia, W. Guo, R. Hu, J.D. Poplawsky, G. Sha, Y. Fang, Z. Yan, C. Wang, C. Li, Y. Zhang, S.J. Zinkle, Y. Wang, Effects of temperature on the irradiation responses of Al0.1CoCrFeNi high entropy alloy, Scripta Mater. 144 (Supplement C) (2018) 31–35.
[11] Y. Zhang, G.M. Stocks, K. Jin, C. Lu, H. Bei, B.C. Sales, L. Wang, L.K. Béland, R.E. Stoller, G.D. Samolyuk, M. Caro, A. Caro, W.J. Weber, Influence of chemical disorder on energy dissipation and defect evolution in concentrated solid solution alloys, Nat. Commun. 6 (2015) 8736.
[12] T.-n. Yang, C. Lu, K. Jin, M.L. Crespillo, Y. Zhang, H. Bei, L. Wang, The effect of injected interstitials on void formation in self-ion irradiated nickel containing concentrated solid solution alloys, J. Nucl. Mater. (2017).
[13] M.-R. He, S. Wang, S. Shi, K. Jin, H. Bei, K. Yasuda, S. Matsumura, K. Higashida, I.M. Robertson, Mechanisms of radiation-induced segregation in CrFeCoNi-based single-phase concentrated solid solution alloys, Acta Mater. 126 (2017) 182–193.
[14] D. Chen, Y. Tong, H. Li, J. Wang, Y.L. Zhao, A. Hu, J.J. Kai, Helium accumulation and bubble formation in FeCoNiCr alloy under high fluence He+ implantation, J. Nucl. Mater. 501 (2018) 208–216.
[15] Z. Yan, S. Liu, S. Xia, Y. Zhang, Y. Wang, T. Yang, He behavior in Ni and Ni-based equiatomic solid solution alloy, J. Nucl. Mater. 505 (2018) 200–206.
[16] Z. Zhang, M.M. Mao, J. Wang, B. Gludovatz, Z. Zhang, S.X. Mao, E.P. George, Q. Yu, R.O. Ritchie, Nanoscale origins of the damage tolerance of the high-entropy alloy CrMnFeCoNi, Nat. Commun. 6 (2015) 10143.
[17] L. Mansur, W. Coghlan, Mechanisms of helium interaction with radiation effects in metals and alloys: a review, J. Nucl. Mater. 119 (1) (1983) 1–25.
[18] S.J. Zinkle, G. Was, Materials challenges in nuclear energy, Acta Mater. 61 (3) (2013) 735–758.
[19] J.F. Ziegler, M.D. Ziegler, J.P. Biersack, SRIM–The stopping and range of ions in matter (2010), Nucl. Instrum. Methods Phys. Res. Sect. B Beam Interact. Mater. Atoms 268 (11) (2010) 1818–1823.
[20] R.E. Stoller, M.B. Toloczko, G.S. Was, A.G. Certain, S. Dwaraknath, F.A. Garner, On the use of SRIM for computing radiation damage exposure, Nucl. Instrum. Methods Phys. Res. Sect. B Beam Interact. Mater. Atoms 310 (2013) 75–80.
[21] B. Han, J. Wei, Y. Tong, D. Chen, Y. Zhao, J. Wang, F. He, T. Yang, C. Zhao, Y. Shimizu, K. Inoue, Y. Nagai, A. Hu, C.T. Liu, J.J. Kai, Composition evolution of gamma prime nanoparticles in the Ti-doped CoFeCrNi high entropy alloy, Scripta Mater. 148 (2018) 42–46.
[22] J.Y. He, H. Wang, H.L. Huang, X.D. Xu, M.W. Chen, Y. Wu, X.J. Liu, T.G. Nieh, K. An, Z.P. Lu, A precipitation-hardened high-entropy alloy with outstanding tensile properties, Acta Mater. 102 (2016) 187–196.
[23] H. Trinkaus, B.N. Singh, Helium accumulation in metals during irradiation – where do we stand? J. Nucl. Mater. 323 (2–3) (2003) 229–242.
[24] S. Jublot-Leclerc, M.L. Lescoat, F. Fortuna, L. Legras, X. Li, A. Gentils, TEM study of the nucleation of bubbles induced by He implantation in 316L industrial austenitic stainless steel, J. Nucl. Mater. 466 (2015) 646–652.
[25] M.L. Jenkins, M.A. Kirk, Characterisation of Radiation Damage by Transmission Electron Microscopy, CRC Press, 2000.
[26] G.S. Was, Fundamentals of Radiation Materials Science: Metals and Alloys, Springer, 2016.
[27] S. Zinkle, 1.03-Radiation-Induced effects on microstructure, in: Comprehensive Nuclear Materials 1, 2012, pp. 65–98.
[28] G.S. Was, T.R. Allen, J.T. Busby, J. Gan, D. Damcott, D. Carter, M. Atzmon, E.A. Kenik, Microchemistry and microstructure of proton-irradiated austenitic alloys: toward an understanding of irradiation effects in LWR core components, J. Nucl. Mater. 270 (1) (1999) 96–114.
[29] J.M. Cookson, R.D. Carter, D.L. Damcott, M. Atzmon, G.S. Was, Irradiation assisted stress corrosion cracking of controlled purity 304L stainless steels, J. Nucl. Mater. 202 (1) (1993) 104–121.
[30] T.R.A.J.T. Busby, J. Gan, G.S. Was, E.A. Kenik (Eds.), Proceedings of Eighth International Symposium on Environmental Degradation of Materials in Nuclear Power Systems – Water Reactors, American Nuclear Society, LaGrange, IL, 1997, p. 758.
[31] T.A.J. Gan, G.S. Was (Eds.), Proceedings of Materials Research Society, Pittsburgh, 1997, p. 445.
[32] Y. Zhang, Y. Zhuang, A. Hu, J. Kai, C. Liu, The origin of negative stacking fault energies and nano-twin formation in face-centered cubic high entropy alloys, Scripta Mater. 130 (2017) 96–99.
[33] D. Hull, D.J. Bacon, Introduction to Dislocations, Butterworth-Heinemann, 2001.
[34] Z. Wu, H. Bei, G.M. Pharr, E.P. George, Temperature dependence of the mechanical properties of equiatomic solid solution alloys with face-centered cubic crystal structures, Acta Mater. 81 (2014) 428–441.
[35] L. Rémy, A. Pineau, B. Thomas, Temperature dependence of stacking fault energy in close-packed metals and alloys, Mater. Sci. Eng. 36 (1) (1978) 47–63.
[36] X.S. Xie, G.L. Chen, P.J. McHugh, J.K. Tien, Including stacking fault energy into the resisting stress model for creep of particle strengthened alloys, Scripta Metall. 16 (5) (1982) 483–488.
[37] Y.L. Zhao, T. Yang, Y. Tong, J. Wang, J.H. Luan, Z.B. Jiao, D. Chen, Y. Yang, A. Hu, C.T. Liu, J.J. Kai, Heterogeneous precipitation behavior and stacking-fault-mediated deformation in a CoCrNi-based medium-entropy alloy, Acta Mater. 138 (2017) 72–82.